ON/OFF Photoswitching and Thermoinduced Spin Crossover with Cooperative Luminescence in a 2D Iron(II) Coordination Polymer

Subrata Ghosh, Sujit Kamilya, Titas Pramanik, Mathieu Rouzières, Radovan Herchel, Sakshi Mehta, Abhishake Mondal

ON/OFF Photoswitching and Thermoinduced Spin Crossover with Cooperative Luminescence in a 2D Iron(II) Coordination Polymer

Subrata Ghosh, Sujit Kamilya, Titas Pramanik, Mathieu Rouzières, Radovan Herchel, Sakshi Mehta, and Abhishake Mondal*

ABSTRACT: A 2D coordination polymer, $\{[Fe(\mathbf{L})_2(NCSe)_2]\cdot 6MeOH\cdot 14H_2O\}_n$ (**1**; **L** = 2,5-dipyridylethynylene-3,4-ethylenedioxythiophene), has been synthesized based on a redox active luminescence ligand. **1** possesses a 2D [4 × 4] square-grid network where the iron(II) center is in a FeN_6 octahedral coordination environment. **1** displays reversible thermoinduced high-spin (HS; $S = 2$) to diamagnetic low-spin (LS; $S = 0$) ON/OFF spin-state switching with a $T_{1/2}$ value of 150 K. Interestingly, optical reflectivity and photomagnetic studies at 10 K under light irradiation revealed an efficient conversion to a photoinduced metastable HS excited state from a LS ground state. Remarkably, the photoexcited HS state can be reversibly switched ON and OFF by using 625 and 850 nm light-emitting-diode lights. Intriguingly, the thermal dependence of the luminescence intensity of the maximum emission at 524 nm for **1** shows a minimum at around the spin-crossover (SCO) temperature, indicating a cooperative nature between the SCO and luminescence properties. Theoretical calculations confirmed the above findings.

Spin manipulation in molecules triggered by minute alteration of the external stimulus is an attractive and fascinating topic in quantum science and technology.[1,2] Spin-crossover (SCO) materials represent a significant way for understanding the molecular spintronics, sensors, switches, nanoscale data recording, and storage devices according to their intrinsic bistable property.[3−7] The rational design of a stimuli-responsive multifunctional coordination polymer (CP) by the incorporation of one or more additional cooperative properties, e.g., magnetic, electric, and optical, with the intrinsic properties, e.g., permanent and tunable porosity, versatile structural topologies, and physicochemical properties, has recently gained significant attention.[8−17] In this aspect, the simultaneous incorporation of both SCO and luminescence properties in a CP is challenging but highly attractive because modulation of the luminescence signal can signify low-spin (LS)/high-spin (HS) population during spin-state switching.[18−25] As a successful synthetic strategy to improve cooperativity between SCO and luminescence properties, the direct coupling between the SCO unit and appropriate luminescent organic linkers to form extended structures is significantly important, and it is challenging to interplay such cooperative properties, which have been rarely investigated in 2D multifunctional CPs.

In this aspect, herein we present one 2D CP by introducing $Fe(NCSe)_2$ with a novel 3,4-ethylenedioxythiophene-based ditopic nitrogen-donor ligand **L** (Scheme S1), which exhibits cooperative SCO and luminescence properties along with exciting ON/OFF photoswitching behavior.

The reaction of a methanolic solution of Fe:2NCSe with ligand **L** in dichloromethane (DCM) afforded **1** as red crystals (see Figures S1−S9 for detailed characterization). Variable-temperature X-ray diffraction analyses were performed on a single crystal of **1** at 120 and 200 K, respectively (Tables S1 and S2). **1** crystallizes in the orthorhombic space group *Ccca*. Its structure consists of the neutral molecular motif $[Fe(\mathbf{L})_2(NCSe)_2]_n$ and interstitial methanol (MeOH) and water solvent molecules (Figures 1 and S10). The overall coordination geometry around each iron center is best described by a slightly distorted octahedron with a FeN_6 environment (CShM program;[26] Table S3), where the iron center is coordinated to the four nitrogen-donor atoms of four monodentate **L** ligands and two nitrogen-donor atoms of two $NCSe^-$ coligands. Ligand **L** is also acting as a bridging ligand to connect iron centers to form the extended 2D [4 × 4] square-grid networks (Figure 1).

At 200 K, the average $Fe-N_{Py}$ and $Fe-N_{NCSe}$ bond distances are 2.212 and 2.090 Å respectively, which suggested the HS state of the iron center (Figure S11 and Table S2).[27−29] Upon lowering the temperature to 120 K, the overall structural motif remains unchanged; however, a great difference occurs in the iron(II) coordination sphere. The average $Fe-N_{Py}$ and $Fe-N_{NCSe}$ bond distances reduce to 1.999 and 1.941 Å, respectively (Figure S11 and Table S2), which fall in the range expected for the LS iron(II) ion.[27−29] The coordinated $NCSe^-$ coligands are almost linear [∠N−C−Se = 178.6(7)°]; however, ∠Fe−N−C angles are deviated from linearity [168.4(5)°] at 200 K (Table S2). These values remain almost identical upon lowering of the temperature to 120 K (Table S2). The octahedral distortion parameter Σ value of

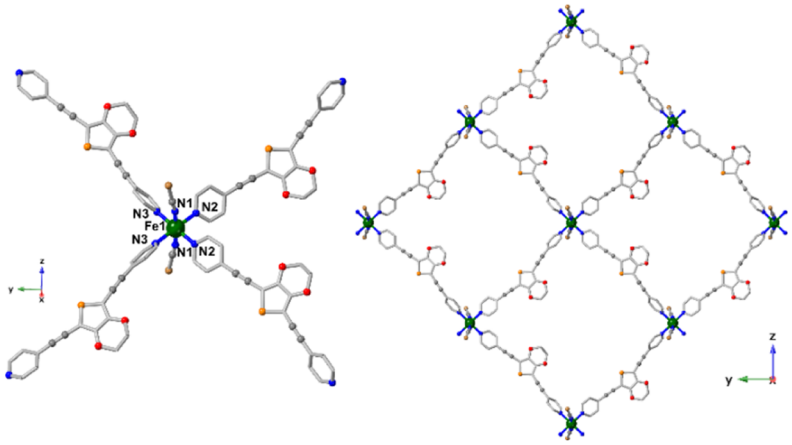

Figure 1. Coordination environment around the iron(II) (left) and 2D network showing a [4 × 4] square grid (right) in **1**. Hydrogen atoms and solvent molecules are omitted for clarity (Fe, green; C, gray; N, blue; O, red; S, orange; Se, brown).

12.8 at 200 K compared to the value of 9.9 at 120 K also suggests the HS state of the iron(II) center at a higher temperature (Table S2),[27−29] supported by CShM analyses (Table S3).

It is worth noting that a contraction in the Fe−N_{py} bond distance of around 0.2 Å is observed, which indicates a complete spin-state switching from the HS to LS state of the iron centers.[27−29] There is a concomitant decrease in the unit cell volume of around 4.5%, the grid diagonal dimension from {28.55 × 28.22} $Å^2$ to {28.00 × 27.72} $Å^2$ and the Fe···Fe length through the bridging **L** ligand from 20.07 to 19.70 Å (Figure S12 and Table S2). Around a 6.7% decrease in the solvent-accessible void volume from 4126.6 to 3851.2 $Å^3$ with a drop from 37.3% to 36.4% of the crystal volume has also been observed.

Magnetic susceptibility measurements were carried out on both fresh crystals kept in a mother liquor (MeOH/DCM/diethyl ether) and a polycrystalline sample of **1** at a magnetic field of 1000 Oe in the temperature range of 2−280 K (Figure 2). The measured χT [χ is magnetic susceptibility equal to M/H per iron(II) ion] value at 280 K is 3.25 cm^3 mol^{-1} K, which lies in the expected range for the iron(II) ion in the HS state (S = 2; g = 2.0; χT = 3.0 cm^3 mol^{-1} K).[27−29] Upon lowering of the temperature, the χT value remains almost constant to 204 K and then decreases gradually to reach a value of 0.15 cm^3 mol^{-1} K at 55 K. The χT value remains almost constant up to 10 K, which indicates a complete and gradual HS-to-LS SCO in **1**.[27−29] In addition, the χT value at 10 K corresponds to less than 2.5% of the residual HS iron(II) center. The small decrease of the χT value below 10 K is probably due to the zero-field splitting of the residual HS iron(II) ion. The field dependence of magnetization studies for **1** were carried out from 0 to 7 T at 1.85, 3, 5, and 8 K (Figure S14). At 1.85 K and 7 T, the magnetization value is 0.11μ_B, which is due to the residual HS iron(II) center, matching well with the χT data. In addition, M versus H/T measurement displays nonsuperposition of the magnetic data on a single master curve, probably is due to the presence of magnetic anisotropy coming from the residual HS iron(II) ion. It is worth mentioning that no out-of-phase (χ'') signal under a zero direct-current field of the alternating-current susceptibility was observed in **1**, confirming the absence of a slow magnetic relaxation phenomenon (Figure S15).

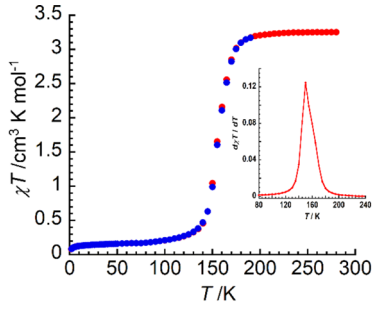

Figure 2. Temperature dependence of the χT product for **1** at 1000 Oe in the cooling (blue) and heating (red) modes. Inset: $d\chi T/dT$ versus T identifies $T_{1/2}$ = 150 K for **1**.

The peak maxima of the $d(\chi T)/dT$ versus T plot in the temperature range of 240−80 K indicate the SCO temperature $T_{1/2}$ at around 150 K in **1**. The identical magnetic responses in both the heating and cooling modes suggest a reversible ON/OFF SCO for **1**. The best fit of the χT versus T data (Figure S16) using the ideal solution model[30] gives the thermodynamic parameters ΔH = 27.9(2) kJ mol^{-1}, $T_{1/2}$ = 155(1) K, and $\Delta S = \Delta H/T_{1/2}$ = 180 J K^{-1} mol^{-1}, which lie in the range expected for the iron(II) SCO systems.[27−29]

Furthermore, optical-reflectivity studies have also been investigated between 270 and 10 K for **1** (Figure S17). Thermal evolution of the absolute reflectivity clearly indicates SCO between the HS and LS states around 150 K, which is very close to the $T_{1/2}$ value.

To explore the photosensitivity of **1**, the sample was irradiated with white light (WL; power = 0.5 mW cm^{-2}) for ca. 100 min at 10 K. The resultant spectrum significantly differs from the spectra obtained in the dark at both 10 and 270 K (Figure S18, left), suggesting the possibility of formation of the HS iron(II) state from the LS state of **1** at 10 K. The evolution of absolute reflectivity versus time exhibits an increase in the absolute-reflectivity value, attaining a saturation after 20 min of WL irradiation (Figure S18, right). This value is matching well with the one obtained at 270 K, which indicates a complete recovery of the HS state and thus suggests a complete photoinduced SCO of **1** from the LS state at 10 K. After irradiation, the thermal stability of the photoinduced metastable HS state was also investigated by heating the sample in the dark (sweep rate = 0.4 K min^{-1}; Figure 3, left),

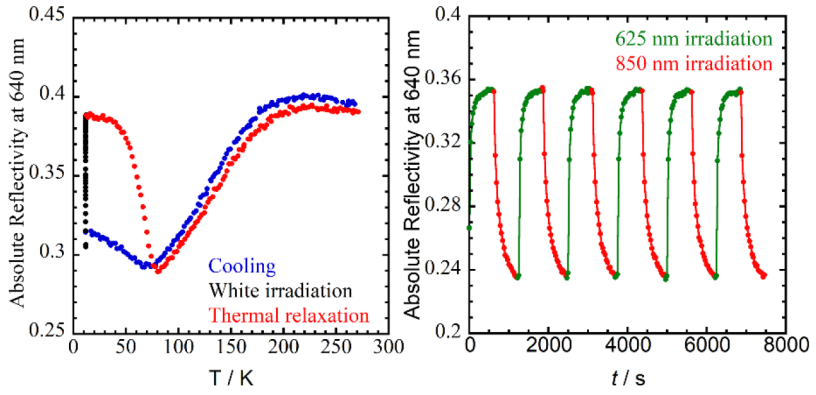

Figure 3. Left: Thermal evolution of the absolute-reflectivity signal plotted at 640 nm in the cooling mode, during WL irradiation (10 K), and in the heating mode for **1**. Right: Time evolution of the absolute reflectivity under successive irradiations by 625 and 850 nm LEDs for **1** at 10 K.

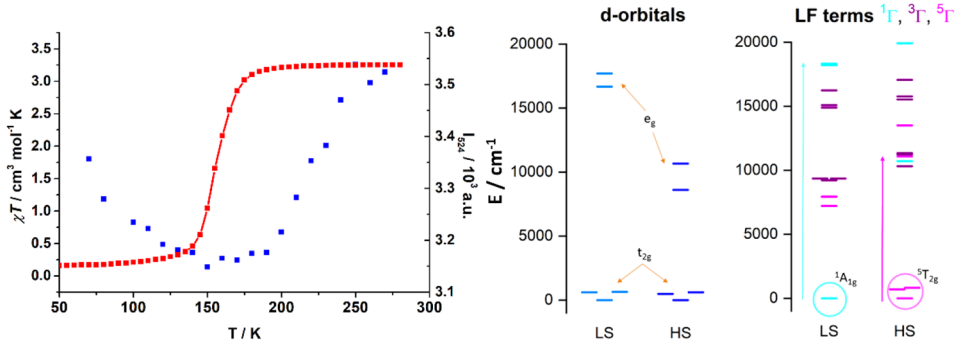

Figure 4. Left: Thermal variation of the luminescence intensity of the maximum emission (λ_{em} = 524 nm) for **1** with a temperature dependence of the χT product. Middle: Splitting of the d orbitals resulting from AILFT analysis of CASSCF/NEVPT2 for **1**. Right: Ligand-field terms resulting from CASSCF/NEVPT2 calculations showing also possible excitation energies to the lowest state with the same multiplicity as the ground state.

which shows a decrease in the absolute reflectivity due to relaxation of the photoinduced HS state to the diamagnetic LS ground state, where a complete relaxation was observed at around 80 K (T_{LIESST}). After this temperature, the absolute-reflectivity values show a feature similar to that observed in the dark. Additional photoexcitation at 10 K with 14 light-emitting diodes (LEDs; 1050−365 nm) showed that all LEDs were able to populate the paramagnetic HS state (Figure S19), in agreement with the efficiency of WL,[31−33] where a maximum efficiency was observed for 625 nm. Accordingly, further photoexcitation studies were carried out with 625 nm LED irradiation at 10 K, which led to similar outcomes (Figures S20 and S21). Interestingly, a weak time relaxation of the photoinduced metastable state in the dark at 10 K can be seen mainly in the first 5 min (Figure S22), which becomes very slow afterward. The effect of the irradiation power was also studied for the most efficient LED, i.e., 625 nm (Figure S22), and when the power is increased, the saturation value is slightly higher and is reached relatively faster, which can be ascribed to a better light penetration at the surface of the sample.

Further optical-reflectivity studies with LED lights were carried out at 10 K by cycling photoexcitation at 625 nm (30 min; power = 16 mW cm^{-2}) and a second irradiation with other LEDs to explore the possibility of photoreversibility of **1**. The most significant changes in the spectra were observed with the 940−780 nm LEDs, as expected for the HS-to-LS photoconversion (Figure S23) for the iron(II) system. Accordingly, further deexcitation studies were carried out with 850 nm LED irradiation at 10 K. During 850 nm LED irradiation, a drop of the absolute-reflectivity data was observed (Figure S24, left). Interestingly, the resulting spectrum significantly differs from the spectrum obtained after 625 nm LED irradiation at 10 K. It is worth noting that the spectrum obtained after 850 nm LED irradiation is almost similar to the spectrum at 10 K in the dark (Figure S24, right), indicating the possibility of photodeexcitation of the metastable HS state to the LS state for **1**. After irradiation, an increase of the temperature produced an augment of the reflectivity due to relaxation of the photodeexcitation state. Such an upturn was observed until 80 K. As expected, the data obtained after this temperature exhibit behavior similar to that in the dark. The HS and LS states can thus be reversibly and efficiently ON/OFF switched by using 625 and 850 nm irradiation over several cycles (Figure 3, right) at 10 K. (Photo)magnetic measurements at 10 K under different diode lasers also confirm the above findings (Figure S25).

To find a correlation between the interesting SCO and luminescence properties in **1**, variable-temperature fluorescence measurements were carried out from 270 to 70 K. The ligand **L** shows an emission band centered at around 565 nm upon excitation with 365 nm at room temperature (Figure S26). **1** exhibit a very interesting luminescence property, showing two broad bands centered at 524 and 570 nm upon excitation at 395 nm (Figure S27), which indicates that the luminescence property for **1** is different from that of the ligand albeit with a decreased intensity. As seen in Figure 4 (left), upon a decrease in the temperature, the luminescence intensity

of the maximum emission at 524 nm (I_{524}) initially decreased and then reached the lowest value at around 150 K. Upon a further decrease in the temperature, the emission intensity I_{524} started to gradually increase up to 70 K. Minimization of I_{524} at around the SCO temperature ($T_{1/2}$) of 150 K suggested modulation of the luminescence properties with a thermal population of the HS and LS states. The results conclude a remarkable synergistic correlation between the SCO and luminescence properties in **1**.

A detailed theoretical CASSCF/NEVPT2 calculation[34] revealed the ligand-field strength ($10\ Dq^{LS}/10\ Dq^{HS} \approx 1.81$) and excitation energies for light-induced excited spin-state trapping (LIESST; $^1\Gamma \rightarrow {}^1\Gamma^*$; $\Delta\varepsilon^{LS} \approx 18217\ cm^{-1}$) and reverse LIESST ($^5\Gamma \rightarrow {}^5\Gamma^*$; $\Delta\varepsilon^{HS} \approx 11089\ cm^{-1}$; Figure 4), and the role of ligands on the LIESST and reverse LIESST effects in **1** was studied also by time-dependent density functional theory (Figures S29 and S30), confirming the experimental results.

In conclusion, we have successfully prepared a 2D [4 × 4] square-grid iron(II) CP by integrating $Fe(NCSe)_2$ with a redox- and luminescence-active ligand. The CP displayed reversible thermo- and photoinduced ON/OFF spin-state switching. Intriguingly, the temperature dependence of the luminescence measurements confirmed a synergic correlation between the SCO and luminescence properties in **1**. We believe that this work will deliver an important strategy for the design and development of SCO- and luminescence-based magnetooptical materials and open up new ways for the enhancement of smart switchable materials.

AUTHOR INFORMATION

Corresponding Author

Abhishake Mondal − *Solid State and Structural Chemistry Unit, Indian Institute of Science (IISc), Bangalore 560012, India;* orcid.org/0000-0002-5061-2326; Email: mondal@iisc.ac.in

Authors

Subrata Ghosh − *Solid State and Structural Chemistry Unit, Indian Institute of Science (IISc), Bangalore 560012, India;* orcid.org/0000-0003-4539-4413

Sujit Kamilya − *Solid State and Structural Chemistry Unit, Indian Institute of Science (IISc), Bangalore 560012, India;* orcid.org/0000-0003-4881-0638

Titas Pramanik − *Solid State and Structural Chemistry Unit, Indian Institute of Science (IISc), Bangalore 560012, India*

Mathieu Rouzières − *Centre de Recherche Paul Pascal, University of Bordeaux, UMR 5031, CNRS, Pessac 33600, France;* orcid.org/0000-0003-3457-3133

Radovan Herchel − *Department of Inorganic Chemistry, Faculty of Science, Palacký University, Olomouc CZ-771 46, Czech Republic;* orcid.org/0000-0001-8262-4666

Sakshi Mehta − *Solid State and Structural Chemistry Unit, Indian Institute of Science (IISc), Bangalore 560012, India;* orcid.org/0000-0002-1232-4489

ACKNOWLEDGMENTS

This research work is supported by the IISc, Bangalore, India, and the Science and Engineering Research Board (Project SRG/2019/000317). R.H. acknowledges financial support from institutional sources of the Department of Inorganic Chemistry, Palacký University Olomouc, Czech Republic. S.K. thanks the Council of Scientific & Industrial Research (CSIR), Government of India, and S.G. and S.M. thank the IISc for fellowships.

REFERENCES

(1) Coronado, E. Molecular magnetism: from chemical design to spin control in molecules, materials and devices. *Nat. Rev. Mater.* **2020**, *5*, 87−104.

(2) Zhang, C.; Yao, H.; Nie, Y.-H.; Liang, J.-Q.; Niu, P.-B. Magnetic field manipulation of spin current in a single-molecule magnet tunnel junction with two-electron Coulomb interaction. *AIP Adv.* **2018**, *8*, 045309−045317.

(3) Sato, O. Dynamic molecular crystals with switchable physical properties. *Nat. Chem.* **2016**, *8*, 644−656.

(4) Meng, Y.-S.; Liu, T. Manipulating Spin Transition To Achieve Switchable Multifunctions. *Acc. Chem. Res.* **2019**, *52*, 1369−1379.

(5) Senthil Kumar, K.; Ruben, M. Emerging trends in spin crossover (SCO) based functional materials and devices. *Coord. Chem. Rev.* **2017**, *346*, 176−205.

(6) Kahn, O.; Martinez, C. J. Spin-Transition Polymers: From Molecular Materials Toward Memory Devices. *Science* **1998**, *279*, 44−48.

(7) Halcrow, M. A. *Spin-crossover materials properties and applications*; John Wiley and Sons, Inc.: Chichester, U.K., 2013.

(8) Minguez Espallargas, G.; Coronado, E. Magnetic functionalities in MOFs: from the framework to the pore. *Chem. Soc. Rev.* **2018**, *47*, 533−557.

(9) Cui, Y.; Li, B.; He, H.; Zhou, W.; Chen, B.; Qian, G. Metal−Organic Frameworks as Platforms for Functional Materials. *Acc. Chem. Res.* **2016**, *49*, 483−493.

(10) Kitagawa, S.; Kitaura, R.; Noro, S.-i. Functional Porous Coordination Polymers. *Angew. Chem., Int. Ed.* **2004**, *43*, 2334−2375.

(11) Halder, G. J.; Kepert, C. J.; Moubaraki, B.; Murray, K. S.; Cashion, J. D. Guest-Dependent Spin Crossover in a Nanoporous Molecular Framework Material. *Science* **2002**, *298*, 1762−1765.

(12) Qiu, Y.-R.; Cui, L.; Cai, P.-Y.; Yu, F.; Kurmoo, M.; Leong, C. F.; D'Alessandro, D. M.; Zuo, J.-L. Enhanced dielectricity coupled to spin-crossover in a one-dimensional polymer iron(ii) incorporating tetrathiafulvalene. *Chem. Sci.* **2020**, *11*, 6229−6235.

(13) Rice, A. M.; Martin, C. R.; Galitskiy, V. A.; Berseneva, A. A.; Leith, G. A.; Shustova, N. B. Photophysics Modulation in Photoswitchable Metal−Organic Frameworks. *Chem. Rev.* **2020**, *120*, 8790.

(14) Garg, S.; Schwartz, H.; Kozlowska, M.; Kanj, A. B.; Müller, K.; Wenzel, W.; Ruschewitz, U.; Heinke, L. Conductance Photoswitching

of Metal−Organic Frameworks with Embedded Spiropyran. *Angew. Chem., Int. Ed.* **2019**, *58*, 1193−1197.
(15) Feng, J.; Xu, Z.; Dong, P.; Yu, W.; Liu, F.; Jiang, Q.; Wang, F.; Liu, X. Stimuli-responsive multifunctional metal−organic framework nanoparticles for enhanced chemo-photothermal therapy. *J. Mater. Chem. B* **2019**, *7*, 994−1004.
(16) Yao, Z.-Q.; Xu, J.; Zou, B.; Hu, Z.; Wang, K.; Yuan, Y.-J.; Chen, Y.-P.; Feng, R.; Xiong, J.-B.; Hao, J.; Bu, X.-H. A Dual-Stimuli-Responsive Coordination Network Featuring Reversible Wide-Range Luminescence-Tuning Behavior. *Angew. Chem., Int. Ed.* **2019**, *58*, 5614−5618.
(17) Li, Z.-Y.; Dai, J.-W.; Damjanović, M.; Shiga, T.; Wang, J.-H.; Zhao, J.; Oshio, H.; Yamashita, M.; Bu, X.-H. Structure Switching and Modulation of the Magnetic Properties in Diarylethene-Bridged Metallosupramolecular Compounds by Controlled Coordination-Driven Self-Assembly. *Angew. Chem., Int. Ed.* **2019**, *58*, 4339−4344.
(18) Jiao, Y.; Zhu, J.; Guo, Y.; He, W.; Guo, Z. Synergetic effect between spin crossover and luminescence in the $[Fe(bpp)_2][BF_4]_2$ (bpp = 2,6-bis(pyrazol-1-yl)pyridine) complex. *J. Mater. Chem. C* **2017**, *5*, 5214−5222.
(19) Estrader, M.; Salinas Uber, J.; Barrios, L. A.; Garcia, J.; Lloyd-Williams, P.; Roubeau, O.; Teat, S. J.; Aromi, G. A Magneto-optical Molecular Device: Interplay of Spin Crossover, Luminescence, Photomagnetism, and Photochromism. *Angew. Chem., Int. Ed.* **2017**, *56*, 15622−15627.
(20) Benaicha, B.; Van Do, K.; Yangui, A.; Pittala, N.; Lusson, A.; Sy, M.; Bouchez, G.; Fourati, H.; Gomez-Garcia, C. J.; Triki, S.; Boukheddaden, K. Interplay between spin-crossover and luminescence in a multifunctional single crystal iron(ii) complex: towards a new generation of molecular sensors. *Chem. Sci.* **2019**, *10*, 6791−6798.
(21) Yuan, J.; Wu, S. Q.; Liu, M. J.; Sato, O.; Kou, H. Z. Rhodamine 6G-Labeled Pyridyl Aroylhydrazone Fe(II) Complex Exhibiting Synergetic Spin Crossover and Fluorescence. *J. Am. Chem. Soc.* **2018**, *140*, 9426−9433.
(22) Wang, J. L.; Liu, Q.; Meng, Y. S.; Liu, X.; Zheng, H.; Shi, Q.; Duan, C. Y.; Liu, T. Fluorescence modulation via photoinduced spin crossover switched energy transfer from fluorophores to Fe(II) ions. *Chem. Sci.* **2018**, *9*, 2892−2897.
(23) Lochenie, C.; Schötz, K.; Panzer, F.; Kurz, H.; Maier, B.; Puchtler, F.; Agarwal, S.; Köhler, A.; Weber, B. Spin-Crossover Iron(II) Coordination Polymer with Fluorescent Properties: Correlation between Emission Properties and Spin State. *J. Am. Chem. Soc.* **2018**, *140*, 700−709.
(24) Meneses-Sánchez, M.; Piñeiro-López, L.; Delgado, T.; Bartual-Murgui, C.; Muñoz, M. C.; Chakraborty, P.; Real, J. A. Extrinsic vs. intrinsic luminescence and their interplay with spin crossover in 3D Hofmann-type coordination polymers. *J. Mater. Chem. C* **2020**, *8*, 1623−1633.
(25) Delgado, T.; Meneses-Sánchez, M.; Piñeiro-López, L.; Bartual-Murgui, C.; Muñoz, M. C.; Real, J. A. Thermo- and photo-modulation of exciplex fluorescence in a 3D spin crossover Hofmann-type coordination polymer. *Chem. Sci.* **2018**, *9*, 8446−8452.
(26) Casanova, D.; Llunell, M.; Alemany, P.; Alvarez, S. The Rich Stereochemistry of Eight-Vertex Polyhedra: A Continuous Shape Measures Study. *Chem. - Eur. J.* **2005**, *11*, 1479−1494.
(27) Sciortino, N. F.; Neville, S. M. Two-Dimensional Coordination Polymers with Spin Crossover Functionality. *Aust. J. Chem.* **2014**, *67*, 1553−1562.
(28) Mondal, A.; Li, Y.; Chamoreau, L.-M.; Seuleiman, M.; Rechignat, L.; Bousseksou, A.; Boillot, M.-L.; Lescouëzec, R. Photo- and thermo-induced spin crossover in a cyanide-bridged $\{Mo^{V}_{2}Fe^{II}_{2}\}$ rhombus molecule. *Chem. Commun.* **2014**, *50*, 2893−2895.
(29) Mondal, A.; Li, Y.; Herson, P.; Seuleiman, M.; Boillot, M.-L.; Rivière, E.; Julve, M.; Rechignat, L.; Bousseksou, A.; Lescouëzec, R. Photomagnetic effect in a cyanide-bridged mixed-valence $\{Fe^{II}_{2}Fe^{III}_{2}\}$ molecular square. *Chem. Commun.* **2012**, *48*, 5653−5655.
(30) Slichter, C. P.; Drickamer, H. G. Pressure-Induced Electronic Changes in Compounds of Iron. *J. Chem. Phys.* **1972**, *56*, 2142−2160.
(31) Aguilà, D.; Prado, Y.; Koumousi, E. S.; Mathonière, C.; Clérac, R. Switchable Fe/Co Prussian blue networks and molecular analogues. *Chem. Soc. Rev.* **2016**, *45*, 203−224.
(32) Ababei, R.; Pichon, C.; Roubeau, O.; Li, Y.-G.; Bréfuel, N.; Buisson, L.; Guionneau, P.; Mathonière, C.; Clérac, R. Rational Design of a Photomagnetic Chain: Bridging Single-Molecule Magnets with a Spin-Crossover Complex. *J. Am. Chem. Soc.* **2013**, *135*, 14840−14853.
(33) Kamilya, S.; Ghosh, S.; Li, Y.; Dechambenoit, P.; Rouzières, M.; Lescouëzec, R.; Mehta, S.; Mondal, A. Two-Step Thermoinduced Metal-to-Metal Electron Transfer and ON/OFF Photoswitching in a Molecular $[Fe_2Co_2]$ Square Complex. *Inorg. Chem.* **2020** DOI: 10.1021/acs.inorgchem.0c02053.
(34) Neese, F. Software update: the ORCA program system, version 4.0. *Wiley Interdiscip. Rev.: Comput. Mol. Sci.* **2018**, *8*, e1327.